ORIGINAL PAPER

Surface-enhanced Raman scattering in nanoliter droplets: towards high-sensitivity detection of mercury (II) ions

Guoqing Wang · Chaesung Lim · Lingxin Chen · Hyangah Chon · Jaebum Choo · Jongin Hong · Andrew J. deMello

Abstract We report a new method for the trace analysis of mercury (II) ions in water. The approach involves the use of droplet-based microfluidics combined with surface-enhanced Raman scattering (SERS) detection. This novel combination provides both fast and sensitive detection of mercury (II) ions in water. Specifically, mercury (II) ion detection is performed by using the strong affinity between gold nanoparticles and mercury (II) ions. This interaction causes a change in the SERS signal of the reporter molecule rhodamine B that is a function of mercury (II) ion concentration. To allow both reproducible and quantitative analysis, aqueous samples are encapsulated within nanoliter-sized droplets. Manipulation of such droplets through winding microchannels affords rapid and efficient mixing of the contents. Additionally, *memory effects*, caused by the precipitation of nanoparticle aggregates on channel walls, are removed since the aqueous droplets are completely isolated by a continuous oil phase. Quantitative analysis of mercury (II) ions was performed by calculating spectral peak area of rhodamine B at 1,647 cm^{-1}. Using this approach, the calculated concentration limit of detection was estimated to be between 100 and 500 ppt. Compared with fluorescence-based methods for the trace analysis of mercury (II) ions, the detection sensitivities were enhanced by approximately one order of magnitude. The proposed analytical method offers a rapid and reproducible trace detection capability for mercury (II) ions in water.

G. Wang · C. Lim · L. Chen · H. Chon · J. Choo (✉)
Department of Applied Chemistry, Hanyang University,
Ansan 426-791, South Korea
e-mail: jbchoo@hanyang.ac.kr

J. Hong · A. J. deMello
Department of Chemistry, Imperial College London,
South Kensington,
London SW7 2AZ, UK

Introduction

Environmental pollution by heavy metals and the resulting adverse effects on human health are problems of increasing concern [1]. In particular, mercury (II) (Hg^{2+}) is widely considered to be one of the most toxic pollutants [2]. For example, methyl mercury is formed from inorganic mercury by bacteria living in the sediments of aqueous environments. This potent neurotoxin is being cumulative through aquatic food chains resulting in significant body burdens of mercury in humans [3]. The injection of methyl mercury can cause irreversible damage to the central nervous system manifested by the loss of sensory, motor, and cognitive operations, and exposure of high Hg levels can be fatal as well [4–6]. Accordingly, there is a pressing need to develop a fast and sensitive method for the trace analysis of mercury (II) ions in water. To date, different types of analytical methods including atomic absorption spectroscopy, inductively coupled plasma–atomic emission spectrometry, gas chromatography–inductively coupled plasma–mass spectrometry, and selective cold vapor atomic fluorescence spectroscopy have been employed for the detection of mercury (II) ions in a variety of environments [7–10]. Such analytical methods provide limits of detection (LOD) at the parts-per-billion level. Unfortunately, extensive sample preparation, preconcentration times, and analysis times make them less attractive for use in both laboratory and in-the-field environments.

Recently, methods involving gold nanoparticles (AuNPs) have been used to perform trace analysis of mercury (II)

ions in water [11–19]. For instance, the strong affinity between AuNPs and mercury (II) ions causes significant changes in the optical properties of AuNPs. This obviates the need for complex separation or preconcentration of the original sample. Functionalized AuNPs have been employed in both absorption and fluorescence-based assays for the quantitation of mercury (II) ions in water. Indeed, AuNPs, modified with mercaptopropanoic acid [11], oligo-nucleotides [12–15], and peptides [16] have been used to control and modify aggregation properties in colorimetric detection. Moreover, AuNPs functionalized with organic chromophores [17–19] have been used to facilitate fluorescence detection. Interestingly, Huang and Chang reported an elegant approach for determining mercury (II) ions in tap water incorporating the fluorescence quenching of rhodamine B (RB) in the presence of AuNPs [17]. When highly fluorescent RB molecules are adsorbed onto the surfaces of AuNP, their fluorescence quantum yield is reduced by energy transfer phenomena. In the presence of mercury (II) ions, RB molecules are released from the AuNP surfaces and thus restore the original levels of fluorescence emission. In this way, the concentration of mercury (II) ions could be determined with na LOD of approximately 2 ppb. However, there is still a need for new sensitive and rapid assays for mercury (II) ions in water. To this end, surface-enhanced Raman scattering (SERS) is a promising alternative for high-sensitivity analysis of mercury (II) ions. Indeed, when small fluorescent molecules (such as RB) are adsorbed on AuNPs, their SERS signals are strongly increased due to electromagnetic and chemical enhancement factors [20, 21]. However, when in the presence of mercury (II) ions, a proportion of these molecules are released from the metal surface causing a decrease in the observed SERS signal. In contrast to the fluorescence methods, the concentration of mercury (II) ions can be directly determined by monitoring this decrease in the SERS signal. Additionally, SERS-based detection is ideally suited to the simultaneous detection of metal ions since spectroscopic bands are sharp and easily resolvable [22, 23]. However, quantitative trace analysis using SERS has been hindered due to the difficulties associated with reproducing experimental parameters, such as the degree of aggregation, particle size distributions of the metal colloids and the inhomogeneous distribution of molecules on the nanoparticle surface. The implementation of microfluidic techniques has recently been shown to address some of these issues [24–28]. Microfluidic systems possess several advantages over conventional macroscale environments when performing SERS. For example, the ability to operate within a continuous flow regime and the ability to generate homogeneous mixing conditions within microfluidic channels have been shown to engender quantitative SERS-based analysis [25, 27]. However, it is significant to note that the deposition of nanoparticle aggregates on channel surfaces (the *memory effect*) is ameliorated in the high surface-to-volume ratio environments typical of microfluidic systems, thus affecting both sensitivity and reproducibility. To address this issue in part, Popp and coworkers have employed a two-phase liquid/liquid segmented flow system in SERS measurements to good effect [29, 30]. Droplet-based microfluidic systems have gained increasing popularity in recent years. Such systems allow the generation and manipulation of monodisperse nanoliter-sized liquid droplets within an immiscible carrier fluid in a high-throughput manner [31–35]. Compared to single-phase flow, the localization of reagents within discrete and encapsulated droplets enhances mixing, minimizes residence time distributions, and affords ultrahigh analytical throughput [36]. Importantly, the formed droplets may be fused [37], subdivided, sorted [38], isolated, or incubated [39], allowing complex chemical/biological processing in an automated fashion. However, to become a core instrumental platform, high-sensitivity online droplet detection remains a significant challenge. Herein, we demonstrate the use of SERS detection for the highly sensitive trace analysis of mercury (II) ions in water within a droplet-based microfluidic system. Specifically, aqueous droplets containing mercury (II) ions and RB-adsorbed AuNPs act as individual reaction vessels.

Materials and methods

Preparation of dye-labeled gold nanoparticles

Monodisperse aqueous AuNPs were prepared using the process developed by Frens [40]. In brief, a 0.6 mL of 1% trisodium citrate dihydrate (Na_3citrate) solution was added to a 100-mL solution of boiling 0.01% gold chloride trihydrate ($HAuCl_4 \cdot 3H_2O$). The mixture was boiled for 15 min and then cooled to room temperature. UV/Vis absorption analysis estimated the average diameter of gold particles to be 60 nm at a concentration of 0.04 nM. The Raman-active reporter, RB, was adsorbed onto the nanoparticle surfaces by dissolution in 5 mL of the gold nanocolloid solution. RB-adsorbed AuNPs were left for 2–3 h without disturbance.

Microfluidic device fabrication

Microfluidic devices were fabricated in polydimethylsiloxane (PDMS) using standard soft lithographic techniques [41]. PDMS base and curing agent (Sylgard 184, Dow Corning) were mixed in a ratio of 10:1*w/w*, degassed and decanted onto a Silicon master. The resulting structure was cured in an oven and then the structured layer was peeled off from the

master. After punching inlet and outlet holes for fluidic access, the structured PDMS substrate was bonded to a thin cover glass slide. Figure 1a shows a schematic of the microfluidic device used in this work. The five dashed rectangles denote positions at which SERS measurements were made. The main channel and the two side channels were 150 μm wide and 100 μm deep.

SERS detection

Figure 1b displays an optical arrangement for laser focusing on a microdroplet in the PDMS device. SERS measurements were performed using a Renishaw 2000 Raman microscope system. A Melles Griot He–Ne laser operating at $\lambda =$ 632.8 nm was used as the excitation source at a power of approximately 30 mW. The Rayleigh line was removed from the collected Raman signal using a holographic notch filter located in the collection path. Raman scattering was measured using a charge-coupled device (CCD) camera with a spectral resolution of 4 cm^{-1}. An additional CCD camera was fitted to an optical microscope to obtain optical images.

Results and discussion

Figure 2 illustrates the sequential adsorption of RB and mercury (II) ions onto the surface of AuNPs. When RB molecules are added to the gold nanoparticle solution, they adsorb via electrostatic interaction. A fluorescent dye such as RB possesses a large fluorescence quantum efficiency in bulk solution. However, this is drastically diminished via energy transfer when adsorbed on the surface of AuNPs

[17]. In the presence of mercury (II) ions, RB molecules are released from the surface of AuNPs via competitive adsorption, thus generating an increase in the observed fluorescence. By monitoring this signal enhancement, a highly sensitive method for mercury (II) detection can be realized. Several studies using this spectroscopic method have been reported and yield detection limits as low as 2 ppb [17–19]. Such a LOD satisfies the maximum permitted mercury (II) levels in drinking water set by the US Environmental Protection Agency [42].

Nevertheless, SERS detection methods can also be used for the quantitative determination of mercury (II) ions in water. When RB molecules are adsorbed on AuNPs, aggregated clusters are produced and the SERS signal is significantly enhanced by hot spots. To evaluate the degree of aggregation, the extinction spectra for AuNPs and RB-modified AuNPs were measured. Here, absorption due to aggregated AuNPs (ranging from 650 to 800 nm) was observed to increase but the absorption due to single AuNPs (at 535 nm) was seen to slightly decrease. This means that the addition of RB molecules induces aggregation of AuNPs. Conversely, it was previously reported that the addition of mercury (II) ions induces a negligible effect on RB-modified AuNP aggregation [17]. Thus, the reduction of the SERS signal only depends on the decrease in the number of RB molecules. In contrast to the enhancement of the fluorescence signals caused by the replacement of RB molecules by mercury (II) ions, the SERS signals gradually decrease with an increase in mercury (II) ion concentration. This is because the number of Raman reporter molecules adsorbed on the nanoparticle surface decreases within increasing mercury (II) ion concentration.

Fig. 1 a Schematic representation of the channel pattern used to create droplets; b optical arrangement for focusing the excitation beam into the microchannel network; c photograph of the assembled device in operation
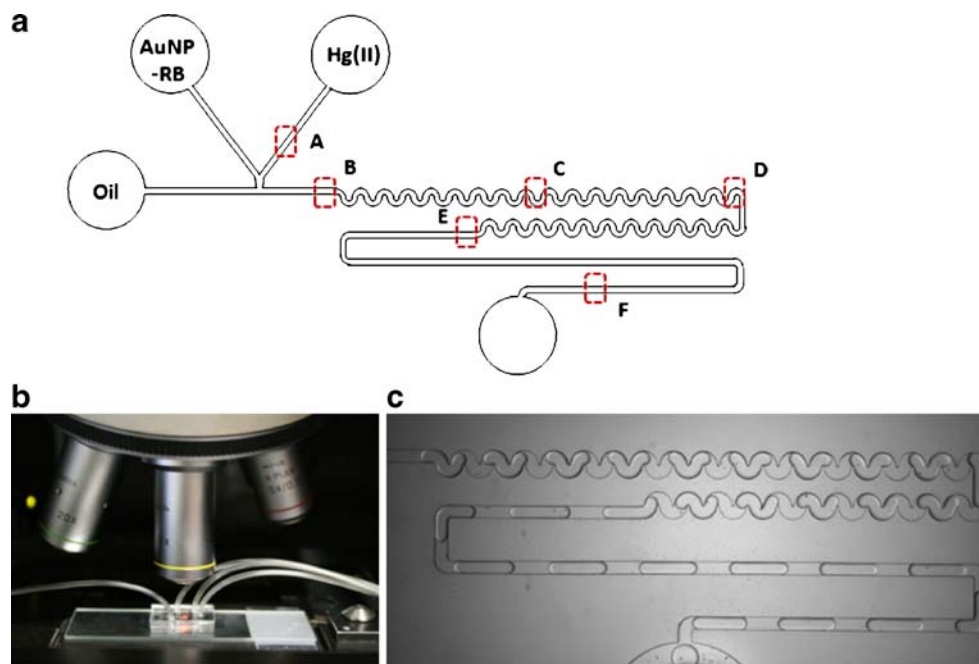
Fig. 2 Schematic representation of the mercury (II) ion sensing mechanism based on the replacement of RB dye molecules through the reduction of mercury (II) ions on the surface of AuNPs
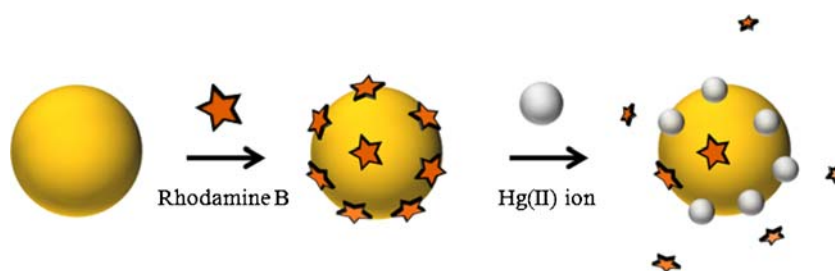

Figure 3 provides a comparison of SERS spectra originating from a sample containing RB-adsorbed AuNPs with the same sample containing 10 ppb of mercury (II) ions. Here, the concentrations of AuNPs and RB were 0.04 and 400 nM, respectively. It can be seen that the SERS intensities are significantly reduced on addition of 10 ppb of mercury (II) ions. This indicates RB molecules have been replaced by the mercury (II) ions. By monitoring this decrease in SERS intensity, quantitative analysis of mercury (II) ions could be achieved. However, in practice, it was difficult to apply this approach for trace analysis because of a lack of control over experimental parameters such as particle size and degree of aggregation [25–27].

To improve system robustness for trace analysis, a droplet-based microfluidic system was used for reagent mixing and fluid control. A schematic illustration of the device structure and operation is provided in Fig. 1. This generic channel geometry was introduced by Ismagilov and provides for efficient droplet generation and mixing of encapsulated reagents [43, 44]. Precision syringe pumps (PHD 2000, Harvard Apparatus) were used to infuse both aqueous solutions and the immiscible carrier fluid at flow rates ranging between 0.1 and 5 µl/min. The aqueous solutions consist of an RB-adsorbed AuNP colloidal solution >and a mercury (II) ion solution (of varying concentration).
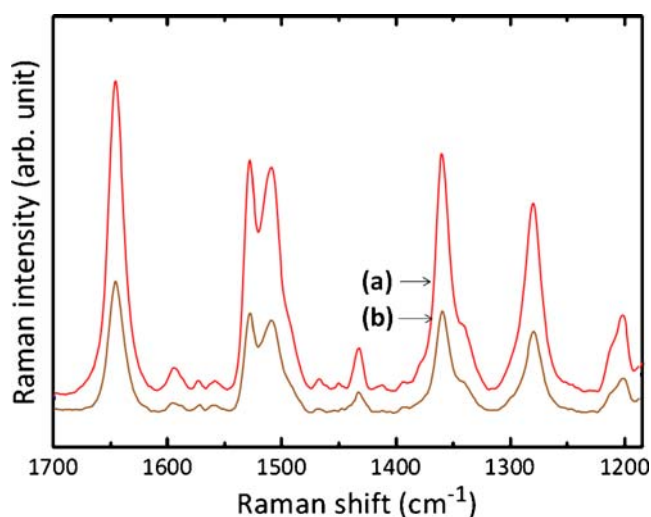

Fig. 3 SERS spectra for **a** RB-AuNPs and **b** the mixture of RB-AuNPs with 10 ppb of mercury (II) ions. The average diameter of AuNPs was estimated to be 60 nm

The carrier fluid is a mixture of perfluorodecalin and 1H,1H,2H,2H-perfluorooctanol (PFO). The two confluent aqueous streams were injected into a stream of flowing carrier fluid where they "bud" into droplets and are transported downstream at a constant velocity by the carrier fluid. The droplet size can be controlled by varying the ratio of the aqueous-to-oil flow rates. Moreover, as droplets pass through the winding channels, efficient mixing is achieved by chaotic advection which acts to stretch, fold, and reorientate contained fluid elements. To find the optimal conditions for the SERS measurements, the flow rates of the aqueous and oil streams were varied between 0.1 and 5.0 µl/min. For the current experiments, the optimum flow rates were determined to be 1.5 µl/min for the carrier oil and 1.0 µl/min for the aqueous stream. Figure 1c shows an image of the microfluidic device in operation at these flow rates. Droplets are formed at the top left-hand part of the photograph and travel downstream at a volumetric flow rate of 1 µl/min. SERS spectra at each channel position were accumulated for 10 s (incorporating the transit of approximately 20 droplets through the detection probe volume). Accordingly, the measured Raman signals include signatures from both the carrier fluid and the RB-adsorbed AuNPs. For the oils used in the current experiments, resulting Raman intensities are negligible compared to the SERS signal of RB-AuNPs.

Figure 4 shows the measured SERS spectra of RB-modified AuNPs and 10 ppb of mercury (II) ions at six different channel positions. The volumetric flow rates of the carrier oil and aqueous flow were 1.5 and 1.0 µl/min, respectively. Positions A, B, C, D, E, and F correspond to the measurement areas depicted in Fig. 3. F′ indicates the Raman spectrum at position F after a period of 5 min under stopped-flow conditions. It can be seen that all major SERS peaks reduce in intensity as a function of distance from droplet formation. This indicates that the aqueous streams of RB-AuNPs and mercury (II) ions are steadily mixed with more mercury (II) ions being adsorbed onto the AuNPs with time. However, the continuous decrease in peak intensity between A and F indicates that this adsorption process does not go to completion. To find equilibrium point of the reaction, a stopped-flow measurement was performed. In this, the flow of the solution was stopped and the SERS signal was measured at 30-s intervals at channel position F. These data indicate that the Raman intensity remains constant after
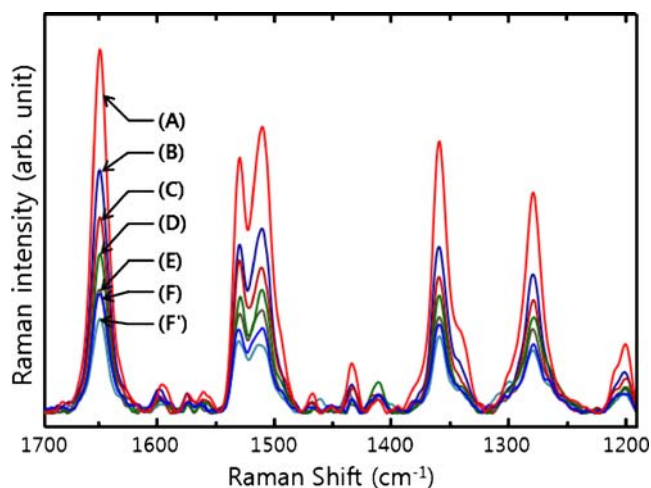
Fig. 4 SERS spectra originating from a confluent mixture of RB-modified AuNPs and 10 ppb of mercury (II) ions at varying positions along the microfluidic channel

5 min (marked as F′ in Fig. 4). Here, the signal intensity at equilibrium F′ corresponds to ~90% of the SERS intensity at position F. Figure 5a displays the change in the characteristic Raman peak of RB at 1,647 cm^{-1} resulting from aqueous droplets containing various concentrations of mercury (II) ions at the position F. The peak intensity decreased concomitantly with the increase in mercury (II) ions, and this peak could be used for the quantitative determination of mercury (II) ions. A fraction of Au bound by mercury (II) ions can be given by

$$[Au - Hg] = 1 - \frac{RA}{RA_{MAX}} \tag{1}$$

where RA and RA_{MAX} represent the peak area at 1,647 cm^{-1} at a concentration of mercury (II) ions and that in the absence of the mercury ions, respectively. [Au–Hg] is plotted as a function of the concentration of mercury (II) ions in Fig. 5b and follows a nonlinear regression model.

$$[Au - Hg] = [Au - Hg]_{MAX} \frac{[Hg^{2+}]}{[Hg^{2+}] + K} \tag{2}$$

where K is the fitting parameter and $[Hg^{2+}]$ is the total concentration of the mercury (II) ions. The nonlinear fit of the data yields $K=1.540$ ppb and $[Au–Hg]_{MAX}=0.5603$. The error bars are the standard deviations from a total of three measurements. A very good linear response in Fig. 5b was found in the concentration range 0.1–2.0 ppb. In addition, the LOD could be determined to be 100–500 ppt, assessed from three standard deviations above the background.

Conclusions

In the present study, a novel method for the trace analysis of mercury (II) ions in water has been developed. SERS

detection, combined with droplet-based microfludics, provides a fast and sensitive detection method. By using the strong affinity between AuNPs and mercury (II) ions, changes in the SERS signal of rhodamine B molecules were monitored. The two-phase segmented system comprises a carrier oil that encapsulates and motivates nanoliter-sized aqueous droplets. Significantly, deleterious *memory effects* previously reported in single-phase microfluidic systems are removed since, although each droplet fills the channel, it does not contact the surface due to presence of a thin layer of the continuous phase. Additionally, efficient and rapid mixing of aqueous fluid elements is realized by chaotic advection (induced by the winding channel geometry). Compared with fluorescence-based methods for the trace analysis of mercury (II) ions, the detection sensitivities were enhanced by approximately one order of magnitude. We expect that our general approach is applicable to the fast and
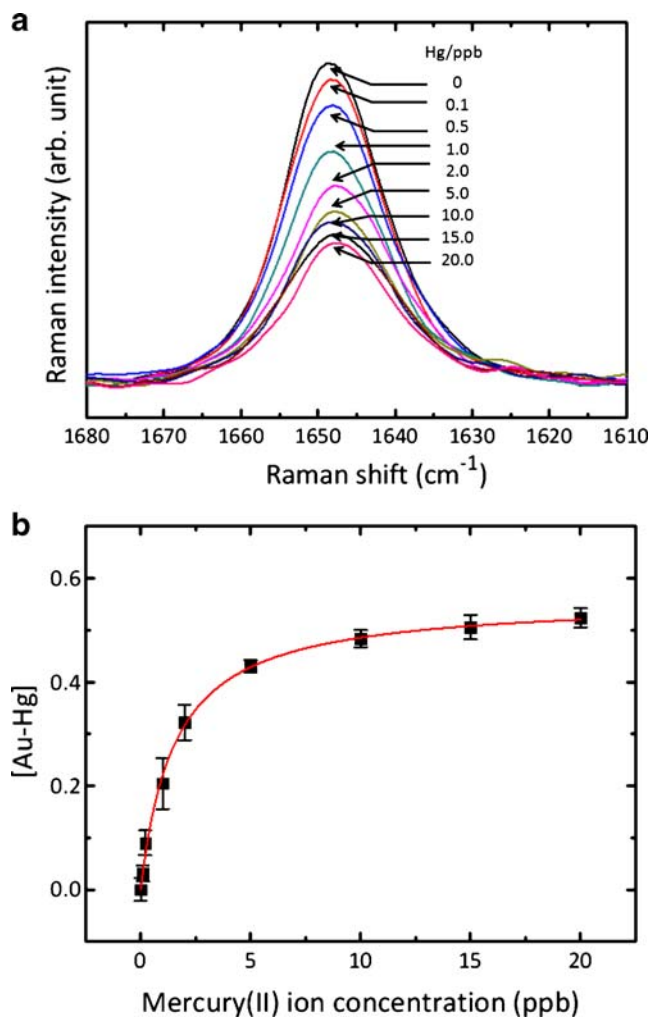

Fig. 5 a Variation of Raman intensity between 1,680 and 1,610 cm^{-1} as a function of mercury (II) ion concentration. All of the spectra were measured at position F; **b** variation of peak area as a function of mercury (II) concentration. *Error bars* denote the standard deviation resulting from three measurements

sensitive trace analyses of other metal ions. Indeed, the use of SERS and droplet-based microfluidics for the multiplexed analysis of metal ions in water is the subject of ongoing studies.

References

1. Campbell LM, Dixon DG, Hecky RE (2003) J Toxicol Environ Health B 6:325–356
2. Sekowski JK, Malkas LH, Wei Y, Hickey RJ (1997) Toxicol Appl Pharmacol 145:268–276
3. Onyido I, Norris AR, Buncel E (2004) Chem Rev 104:5911–5929
4. Reardon AM, Bhat HK (2007) Toxicol Environ Chem 89:535–554
5. Yin Z, Milatovic D, Aschner JL, Syversen T, Rocha JBT, Souza DO, Sidoryk M, Albrecht J, Aschner M (2007) Brain Res 1131:1–10
6. Tamm C, Duckworth J, Hermanson O, Ceccatelli S (2006) J Neurochem 97:69–78
7. Vil'pan YA, Grinshtein IL, Akatove AA, Gucer S (2005) J Anal Chem 60:45–51
8. Butler OT, Cook JM, Harrington CF, Hill SJ, Rieuwerts J, Miles DL (2006) J Anal At Spectrom 21:217–243
9. Li Y, Chen C, Li B, Sun J, Wang J, Gao Y, Zhao Y, Chai Z (2006) J Anal At Spectrom 21:94–96
10. Leemakers M, Baeyens W, Quevauviller P, Horvat M (2005) Trends Anal Chem 24:383–393
11. Huang CC, Chang HT (2007) Chem Commun 1215–1217
12. Chiang CK, Huang CC, Liu CW, Chang HT (2008) Anal Chem 80:3716–3721
13. Liu CW, Hsieh YT, Huang CC, Lin ZH, Chang HT (2008) Chem Commun 2242–2244
14. Lee JS, Han MS, Mirkin CA (2007) Angew Chem Int Ed 46:4093–4096
15. Li D, Wieckowska A, Willner I (2008) Angew Chem Int Ed 47:3927–3931
16. Slocik JM, Zabinski JS Jr, Phillips DM, Naik RR (2008) Small 4:548–551
17. Huang CC, Chang HT (2006) Anal Chem 78:8332–8338
18. Chen J, Zheng AF, Chen AH, Gao Y, He C, Kai X, Wu G, Chen Y (2007) Anal Chim Acta 599:134–142
19. Darbha GK, Ray A, Ray PC (2007) ACS Nano 1:208–214
20. Moskovits M (1985) Rev Mod Phys 57:783–826
21. Otto A, Mrozek I, Grabhorn H, Akemann W (1992) J Phys Cond Matter 4:1143–1212
22. Graham D, Mallinder BJ, Whitcombe D, Smith WE (2002) Anal Chem 74:1069–1074
23. Lee S, Kim S, Choo J, Shin SY, Lee YH, Choi HY, Ha S, Kang K, Oh CH (2007) Anal Chem 79:916–922
24. Quang LX, Lim C, Seong GH, Choo J, Do KJ, Yoo SK (2008) Lab Chip 8:2214–2219
25. Chen L, Choo J (2008) Electrophoresis 29:1815–1828
26. Lee S, Choi J, Chen L, Park B, Kyong JB, Seong GH, Choo J, Lee Y, Shin KH, Lee EK, Joo SW, Lee KH (2007) Anal Chim Acta 590:139–144
27. Park T, Lee S, Seong GH, Choo J, Lee EK, Kim YS, Ji WH, Hwang SY, Gweon DG, Lee S (2005) Lab Chip 5:437–442
28. Jung J, Chen L, Lee S, Kim S, Seong GH, Choo J, Lee EK, Oh CH, Lee S (2007) Anal Bioanal Chem 387:2609–2615
29. Strehle KR, Cialla D, Roesch P, Henkel T, Koehler M, Popp J (2007) Anal Chem 79:1542–1547
30. Ackermann KR, Henkel T, Popp J (2007) ChemPhysChem 8:2665–2670
31. Huebner A, Srisa-Art M, Holt D, Abell C, Hollfelder F, deMello AJ, Edel JB (2007) Chem Commun 1218–1220
32. Srisa-Art M, deMello AJ, Edel JB (2007) Anal Chem 79:6682–6689
33. Srisa-Art M, deMello AJ, Edel JB (2008) Phys Rev Lett 101:014502
34. Huebner A, Olguin LF, Bratton D, Whyte G, Huck WTS, deMello AJ, Edel JB, Abell C, Hollfelder F (2008) Anal Chem 80:3890–3896
35. Huebner A, Sharma S, Srisa-Art M, Hollfelder F, Edel JB, deMello AJ (2008) Lab Chip 8:1244–1254
36. Song H, Tice JD, Ismagilov RF (2003) Angew Chem Int Ed 42:768–772
37. Niu X, Gulati S, Edel JB, deMello AJ (2008) Lab Chip 8:1837–1841
38. Link DR, Gransland-Mongrain E, Duri A, Sarrazin F, Cheng Z, Cristobal G, Marquez M, Weitz DA (2006) Angew Chem 118:2618–2622
39. Courtois F, Olguin LF, Whyte G, Bratton D, Huck WTS, Abell C, Hollfelder F (2008) ChemBioChem 9:439–446
40. Frens G (1973) Nat Phys Sci 241:20–22
41. Beard NP, Edel JB, deMello AJ (2004) Electrophoresis 25:2363–2373
42. US EPA (2001) Mercury update: impact on fish advisories. EPA-823-F-01-011
43. Song H, Ismagilov RF (2003) J Am Chem Soc 125:14613–14619
44. Song H, Bringer MR, Tice JD, Gerdts CJ, Ismagilov RF (2003) Appl Phys Lett 22:4664–4666